ACS SENSORS

pubs.acs.org/acssensors

Article

Optical Carbon Dioxide Detection in the Visible Down to the Single Digit ppm Range Using Plasmonic Perfect Absorbers

Tobias Pohl,* Florian Sterl, Nikolai Strohfeldt, and Harald Giessen*

Cite This: *ACS Sens.* 2020, 5, 2628–2635

Read Online

ACCESS | Metrics & More | Article Recommendations | Supporting Information

ABSTRACT: To tackle climate change and reduce CO_2 emissions, it is important to measure CO_2 output precisely. Even though there are many different techniques, no simple and cheap optical method in the visible is available. This work studies plasmonically enhanced optical carbon dioxide sensors in the visible wavelength range. The sensor samples are based on an inert plasmonic perfect absorber, which can be easily and cheaply fabricated by colloidal etching lithography. A CO_2-sensitive polyethylenimine (PEI) layer is then spin-coated on top to complete the samples. The samples are examined continuously by microspectroscopy during different CO_2 exposures to track spectral changes, particularly the position of the resonance centroid wavelength. The samples exhibit a resonance shift of up to 7 nm, depending on the CO_2 concentration and the temperature. The temperature influences the rise time as well as the sensitive concentration range. The concentration dependence of the resonance shift overall follows the shape of a Langmuir isotherm, which includes a nearly linear relation at lower concentrations and elevated temperatures and a saturating behavior at higher concentrations and lower temperatures. The results indicate that a sensitivity in the full range from 100 vol % to below 1 ppm can be achieved. The samples degenerate in a dry inert atmosphere in a matter of days but are useable over multiple weeks when exposed to humidity and CO_2. The PEI reacts very selectively to CO_2, showing no response to CO, NH_3, NO_2, CH_4, H_2, and only a very small response to O_2. Overall, polyethylenimine is very promising as a CO_2-sensitive material for many practical sensing applications over a wide range of concentrations. An adjustment of the temperature is mandatory to control the sensitivity and response time.

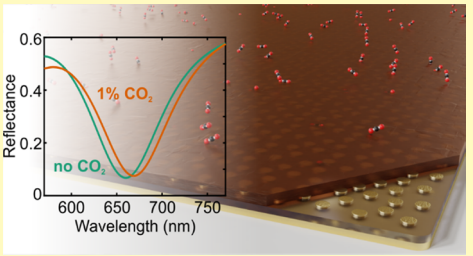

KEYWORDS: *PEI, CO_2, gas sensing, optical, perfect absorber, refractive index sensing, plasmonic sensing*

With a global annual emission of nearly 34 gigatons, CO_2 accounts for three quarters of all greenhouse gases and is one of the main driving forces of climate change.[1] To reduce CO_2 emissions, it is crucial to run combustion processes at conditions that emit the least CO_2. Not only here but also wherever gases occur as precursors (such as in the semiconductor industry), main products (like in the chemical industry), or in any other way, the concentration of these gases needs to be monitored to control the processes and keep up a high efficiency and a steady quality.

In general, gas detection can be carried out by (photo)-acoustic, catalytic, electrical, electrochemical, optical, thermal, and many more methods.[2,3,12,13,4−11] For most of these sensor types, configurations for carbon dioxide are available.[14−19] Optical sensing offers the advantage that the sensing volume can easily be separated from all electronics. This makes this technology superior in areas where electronics are disrupted or pose a safety risk like in explosive environments. Being compliant with, for example, the ATEX directive of the European Union is much easier if an optical sensor is used.[20]

Currently, optical CO_2 sensing is mostly done by using its characteristic infrared absorption values at 1.6, 2.0, 2.7, and 4.3 μm.[21] This method is robust, sensitive, and, due to the specificity of the absorption wavelengths, also very selective but requires a large sensing volume and expensive infrared optics. The sensing scheme used in this paper is based on relatively simple and cheap plasmonic structures that shift their resonance wavelength upon gas exposure. This enables our sensor to offer a high CO_2 sensitivity using visible light and a small sensing volume at moderate temperatures. Furthermore, this scheme allows a simplification and miniaturization of the sensor, reducing the costs significantly.[22]

It was shown in the literature that it is possible to detect hydrogen optically by using plasmonic structures such as a perfect absorber structure incorporating palladium nanostructures on top.[23,24] A plasmonic perfect absorber consists of a metallic mirror below a dielectric spacer and a nanostructured metal layer. The localized surface plasmons of the metal nanostructures in combination with the spacer layer and the metal mirror below form a cavity and create an optical resonance where the reflectance decreases to nearly zero. The resonance wavelength depends on the materials as well as on

Received: June 8, 2020
Accepted: July 22, 2020
Published: July 22, 2020

https://dx.doi.org/10.1021/acssensors.0c01151
ACS Sens. 2020, 5, 2628–2635

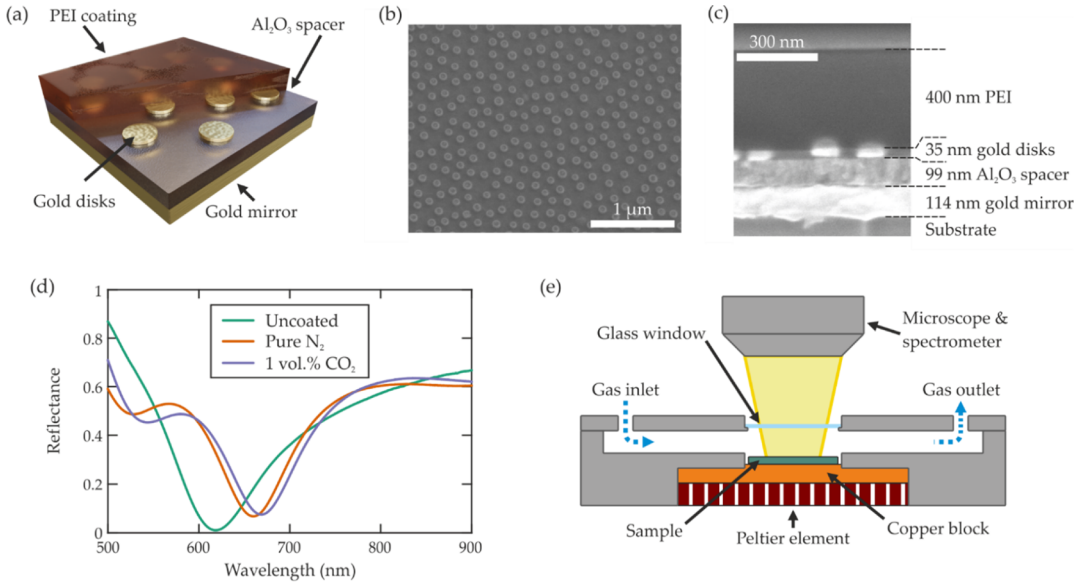

Figure 1. (a) Layout of the samples. PEI is spin-coated on top of an inert perfect absorber, which consists of a gold mirror, an Al_2O_3 spacer layer, and gold nanodisks with an average diameter of 86 nm. (b) SEM picture of the sample without PEI coating at an angle of 15° showing the random but even distribution of the disks. (c) SEM picture of the breaking edge of a ruptured sample, indicating the thickness of the individual layers. The disk layer seems to be thicker than designed due to redeposition of gold during the etching process. The shadow on top of the third disk from the left is some rarely occurring remnant of a polystyrene sphere. (d) Measured reflectance spectra of an uncoated perfect absorber sample and a PEI-coated sample in pure N_2 and in CO_2 diluted in N_2. (e) Gas cell used in the measurements. The top part holds the gas inlet and outlet as well as a glass window to read out the sample optically. The bottom part holds the sample and a Peltier element to control the temperature.

the dimensions of the nanostructures and the dielectric spacer.[25−27]

The reaction of hydrogen with palladium leads to a change in the dielectric function of the palladium and therefore to a shift of the plasmonic resonance, which was shown to work as a sensor.[28,29] To extend this perfect absorber-based gas detection scheme to other substances, alternative materials that react reversibly with these other substances are necessary.

Gas-sensitive metals can be integrated directly into the perfect absorber as the nanostructured top layer. Dielectric materials such as metal oxides or polymers can be integrated either as a spacer layer or, if the fabrication would degenerate them, as an additional coating on top of the metal nanostructures.[30] While the first two options represent direct plasmonic sensing, the latter is termed as indirect plasmonic sensing.[31−33] Polymers containing amines are known to exhibit a response that can be detected: all three types—primary, secondary, and tertiary amines—are able to bind CO_2 reversibly, which changes the refractive index of the polymer. A polymer with a very high density of amines is branched polyethylenimine (PEI). It is a conductive polymer, which not only is widely known and investigated for its reversible CO_2 storage capabilities but can also be used to detect CO_2 electrically and in the infrared.[34−36] In our configuration, PEI was added as a coating on top of an inert perfect absorber using gold nanodisks and an Al_2O_3 spacer. In principle, it is also possible to use PEI as a spacer layer, but here, the PEI would be easily destroyed during the etching of the gold nanodisks. A similar system using nanodisks on a glass substrate and a PIM-1 coating was used by Nugroho et al. to investigate adsorption energetics optically by measuring the resonance shift.[37]

The primary and secondary amines in PEI react with CO_2 by forming carbamates, while tertiary amines react with a different mechanism and form bicarbonates.[38−40]

$$2\,R_1 - NH_2 \rightleftharpoons R_1 - NHCOO^- + R_1 - NH_3^+ \quad (1)$$

$$2\,R_1R_2 - NH + CO_2 \rightleftharpoons R_1R_2 - NCOO^- + R_1R_2 - NH_2^+ \quad (2)$$

$$R_1R_2R_3 - N + H_2O + CO_2 \rightleftharpoons R_1R_2R_3 - N^+ + HCO_3^- \quad (3)$$

While tertiary amines require water to react at all with CO_2, primary and secondary amines can use water to replace one of the two necessary amines in reactions 1 and 2.[41] This means that the CO_2 capacity and therefore the maximum resonance shift can be drastically increased by using humidified gas instead of dry gas.

EXPERIMENTAL METHOD

Sample Fabrication and Characterization. The perfect absorber used in this paper utilizes Al_2O_3 as a spacer material on top of a gold mirror and gold nanodisks as plasmonic structures. The dimensions are based on simulations using an in-house scattering matrix software, defined as a 120 nm-thick gold mirror, a 100 nm-thick Al_2O_3 spacer layer, and gold nanodisks with a diameter of 82 nm and a thickness of 20 nm.[42] Additionally, a PEI layer was spin-coated on top of the perfect absorber (Figure 1a).

The gold mirror, a 100 nm Al_2O_3 spacer layer, and a 20 nm gold layer for the disks were deposited on a cleaned glass substrate in one run by electron beam evaporation. Due to the thin film interferences, the unstructured samples show a bright metallic pink color. The top gold layer was then structured by colloidal etching lithography using 82 nm polystyrene spheres and an etching time of 60 s in an argon ion beam etcher.[43] This method allows us to structure large area samples (here, 1 × 1 cm^2) easily and cheaply in substantial numbers and is therefore directly usable for an industrial scale fabrication. Afterward, the residual polystyrene spheres were removed by oxygen plasma etching. Due to the structuring, a plasmonic resonance at approximately 620 nm with a reflectance of around 1% is present (Figure 1d) and the sample color switches to a deep metallic green. The resulting disks were arranged randomly with a uniform density

https://dx.doi.org/10.1021/acssensors.0c01151
ACS Sens. 2020, 5, 2628−2635

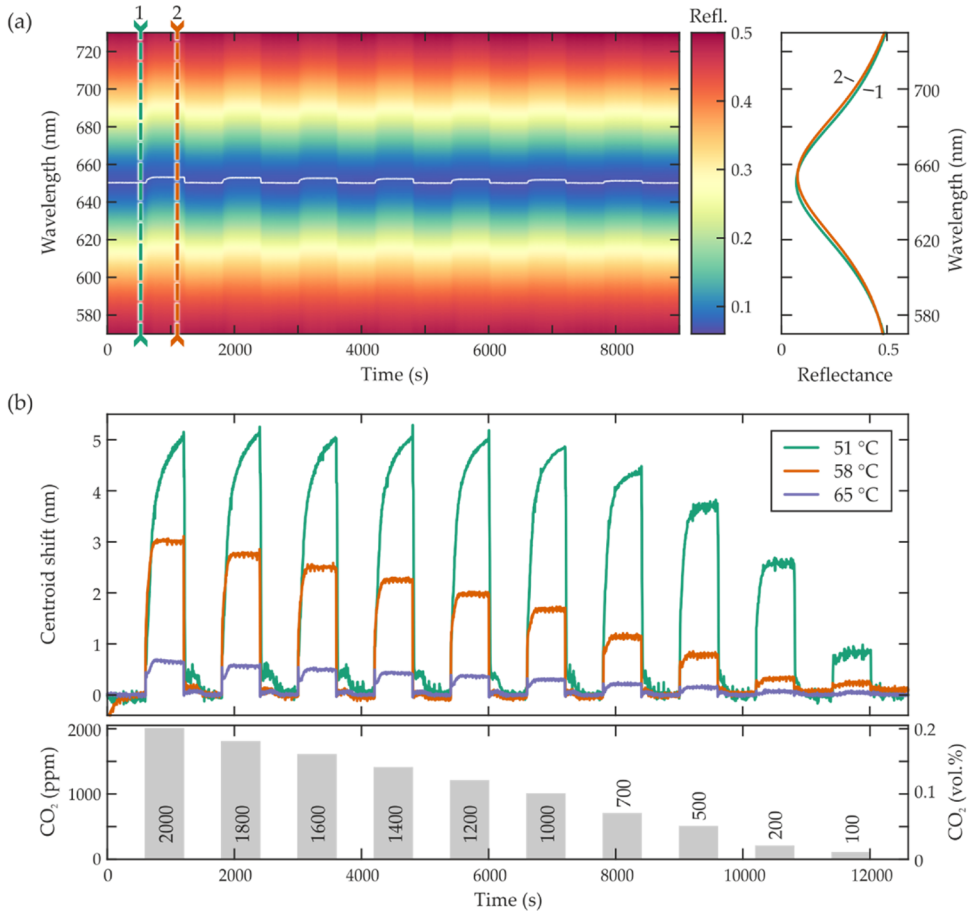

Figure 2. (a) Progression of the reflectance spectrum of a PEI-coated perfect absorber during the gas cycle shown in the bottom of panel (b) at T = 58 °C. The white line shows the centroid wavelength of each individual spectrum, and the inset on the right shows the spectra at pure nitrogen and 0.2 vol % CO_2. (b) Time series of the resonance shift during the gas cycle shown in the bottom at different temperatures. The gas cycle decreases the CO_2 concentration in N_2 stepwise from 0.2 (2000 ppm) to 0.01 vol % (100 ppm) while flushing with pure N_2 between the individual steps.

due to the distribution of the polystyrene spheres (Figure 1b) and possess a mean diameter of 86 nm. The rings on top of the disks result from redeposition of gold beneath the edge of the polystyrene spheres during the ion beam etching. These rings can be avoided by using a sacrificial layer between the gold layer and the spheres or by carefully melting the spheres, but since they do not interfere with the sensing, this step was omitted to keep the fabrication as simple as possible. Pure polyethylenimine (PEI; M_w ~25,000) was purchased from Sigma-Aldrich and diluted in water to 10 wt % solution. To enhance the dissolving, the mixture was stirred for 6 h on a hotplate at 60 °C. The sample surface was first treated by oxygen plasma before 40 μL of PEI (60 °C) was spin-coated at 8000 rpm for 60 s on top of it. Figure 1c displays a cross-sectional scanning electron microscopy (SEM) micrograph of the finished structure, obtained at the breaking edge of a sample. As this image demonstrates, a PEI layer thickness of approximately 400 nm was obtained. This layer red-shifted the resonance wavelength of the perfect absorber structure by approximately 60 nm and increased the minimum reflectance to 7% (Figure 1c).

Measurement Setup. The coated samples were optically characterized and studied in a microspectroscopy setup together with a gas cell (Figure 1e). The microspectroscopy setup consists of a Nikon Eclipse LV100 upright microscope combined with a Princeton Instruments IsoPlane-160 spectrometer and a Pixis 256E camera. The illumination was performed by a laser-driven white light source (Energetiq EQ-99XFC), which is coupled into the microscope. All measurements were carried out with a Nikon TU Plan Fluor 10× objective and unpolarized light. Additionally, a motorized and computer-controlled stage with a μm precision was installed in the sample plane of the microscope to enable an automated measurement process.

The gas cell is custom-designed to fit into the sample holder of the microscope stage. It has a thin glass window above the sample holder for the optical measurements and is equipped with a Peltier element coupled to a copper block but thermally isolated from the rest of the cell to control the temperature of the sample. A Meerstetter Engineering TEC controller was used to keep the temperature constant with less than 0.1 °C deviation. The exact temperature at the sample surface was continuously monitored using an NTC temperature sensor. It should be noted that this precisely tempered and highly stable temperature is only necessary for a full characterization of the sensor. In a real-world application, it is possible to compensate for temperature deviations using appropriate algorithms in combination with the known temperature-dependent behavior.[29]

The gas inlet is connected to a bottle-fed gas mixing system consisting of multiple Bronkhorst mass flow controllers that can regulate the gas flow rate from 2 to 100% of their maximum flow rate at an accuracy of 0.01% as well as a humidifier. The total gas flow rate was kept constant at 1 standard l/min (slm) during each measurement to ensure a constant pressure inside the gas cell. The used gases are Nitrogen 4.8, Protadur (20 vol % CO_2 in N_2), and two custom-mixed test gases with 2000 and 100 ppm CO_2 in N_2. The cross sensitivities were tested by using synthetic air and forming gas (10 vol % H_2 in N_2). All gases were purchased from Westfalen AG. The absolute humidity was kept constant at 0.015 g/L during all measurements.

The entire setup is controlled by a single LabVIEW program that automatically records the reflectance spectra of the sample and a

https://dx.doi.org/10.1021/acssensors.0c01151
ACS Sens. 2020, 5, 2628−2635

reference (usually a gold mirror) at a defined interval while changing the gas mixture according to a given gas cycle. The software also calculates the spectral reflectance of the sample by dividing each sample spectrum by their reference spectrum and then determines the centroid wavelength of the resonance (Figure S1), which has been shown to be more stable than tracking the minimum.[44] Instead of this complex setup and the tracking of the resonance, it is also possible to measure the intensity change at one of the sides of the resonance, reducing the costs of the setup immensely, as recently shown by Herkert et al. (see Figure S7).[22]

SENSING BEHAVIOR

The response of the reflectance spectrum, especially the resonance centroid wavelength, is tracked during different gas cycles at multiple temperatures to study the CO_2 concentration and temperature dependence. The used gas cycles are being switched back and forth between pure nitrogen and a mixture with carbon dioxide while keeping the overall flow rate constant.

Figure 2a shows the development of the reflectance spectrum during a gas cycle with periodically decreasing CO_2 concentrations (shown in Figure 2b) at T = 58 °C. The measurements exhibit a spectral shift every time the gas mixture changes. At wavelengths below 650 nm, the reflectance increases upon CO_2 exposure, while it decreases at wavelengths above 650 nm. A comparison between a spectrum recorded right before the change from pure nitrogen to a nitrogen CO_2 mixture (#1) and one right before switching back (#2) shows that this happens due to a shift of the resonance to higher wavelengths. The tracking of the resonance (centroid) wavelength, which is marked by the white line, shows that this happens at every exposure of the sample to CO_2, even for lower concentrations.

Figure 2b demonstrates the resonance shift during the gas cycle drawn below, which alternates each 600 s between pure nitrogen and a mixture of nitrogen and CO_2. The CO_2 concentration in the mixture is reduced stepwise from 2000 (0.2 vol %) to 100 ppm (0.01 vol %). All three measurements were done on the same spot of the same sample while changing only the temperature. A simple drift correction was applied to the time traces to compensate for systematic drift, such as focal drift or spatial drift of the setup during long measurement cycles (see Figure S3). At T = 51 °C, the first five CO_2 exposures reveal nearly the same maximum shift and still a strong slope at the end of the CO_2 exposure. For a concentration below 1000 ppm, the maximum shift indicates a stronger concentration dependence and the system reaches a state closer to equilibrium during the CO_2 exposure. At 100 ppm, the equilibrium is reached nearly instantaneously. At higher temperatures, a concentration dependence is clearly visible over the entire measured concentration range and the equilibrium is reached much faster than at T = 51 °C. The same holds true for the relaxation after switching back to pure nitrogen: at higher temperatures, the resonance reverts to the base state nearly instantaneously, while this takes a couple of minutes at lower temperatures (see also Figure S5b). The short spikes right before and after the switching of the gas mixture as well as the sometimes increased noise result from instabilities of the humidifier.

The different saturation and relaxations times result from a faster diffusion and an increased reaction rate due to the higher temperatures. Please note that the absorption and desorption of CO_2 in the PEI are different chemical reactions and therefore also differ in their dynamics.[38] To explain the different shifts at the same concentrations but different temperatures, it is necessary to take a closer look at the reaction of the amines and the CO_2. In a simplified form, the reaction is

$$\text{amines} + CO_2 \rightleftharpoons \text{carbamates}$$

Since the reaction is reversible, an equilibrium forms at a specific ratio between amines and carbamates, which depends on a number of different parameters. The influence of a variation of some of these parameters can be predicted by Le Chatelier's principle, which states that a system in equilibrium tries to mitigate the influence of parameter changes by shifting its equilibrium.[45] In the case of a temperature increase, this means that the equilibrium will shift to the endothermic side. The reaction of amines and CO_2 is exothermic, which means that the equilibrium will shift to the left at higher system temperatures and to the right at lower ones. Since the carbamates on the right side of the reaction are responsible for the refractive index change of PEI and therefore directly connected to the resonance shift, this leads to a smaller resonance shift at higher temperatures.

The same principle is responsible for the concentration dependence: if more CO_2 is added to the system by increasing the concentration in the mixture, then the equilibrium shifts to the right to lessen the change, which leads to more carbamates and therefore also to a higher shift. As shown in Figure 2b, it takes the sensor in most cases over 600 s to reach equilibrium at T = 51 °C. At higher concentrations and lower temperatures, this time increases even more; for instance, an exposure of a sample to 5000 ppm (0.5 vol %) CO_2 at 20 °C did not reach equilibrium even after 40 min (Figure S5a). To still be able to estimate reasonable data points here, a simple model of the CO_2 absorption process was developed to extrapolate the resonance shift at equilibrium from the beginning of the time series. This is even more important in real applications as it is often not feasible to wait until a complete saturation is reached. A more sophisticated model for a hydrogen sensor presented by Teutsch et al. proves that it is possible to estimate the gas concentration accurately from the first few seconds of an exposure.[29] Please note that we only consider the CO_2 absorption process in our model as equilibrium is always reached within the recorded desorption period (see Figure 2b), making it unnecessary to extrapolate the time series after decreasing the CO_2 concentration to zero.

The resonance shift depends in the present range of change linearly on the refractive index.[46] On the other hand, it is reasonable to estimate that the change of the refractive index depends linearly on the amount of reacted amines.[47] For nanoporous polymers, this amount follows the shape of a Langmuir isotherm.[35,37,38,48,49] Meanwhile, according to Henry's law, the CO_2 concentration in equilibrium is the same in the entire PEI layer; it is determined by the diffusion of the CO_2 through the PEI otherwise.[49] Therefore, the time dynamics are added by using the CO_2 concentration $c(t)$ in the polymer as the input value for the Langmuir isotherms

$$\Delta\lambda \propto \Delta n \propto \frac{a \cdot c(t)}{1 + b \cdot c(t)}$$

with a and b being fitting parameters, t is the time, and $c(t)$ is given by the solution of the diffusion equation for a plane with constant concentrations on the surface.[50] Details can be found in the Supporting Information.

https://dx.doi.org/10.1021/acssensors.0c01151
ACS Sens. 2020, 5, 2628−2635

Even though the model is able to extrapolate the course of the resonance shift over time upon CO_2 exposure very well (see the Supporting Information, Figure S4), it is still a simplified model and therefore not able to predict the resonance shift at equilibrium completely accurately. Still, it gives a much better grasp of the behavior of the sensor than the data points taken directly from the unsaturated measurements. In case the equilibrium is reached, like in Figure 2b at T = 58 °C, the model matches the measurements nearly perfectly. Figure 3a shows the mean resonance shift that is reached by

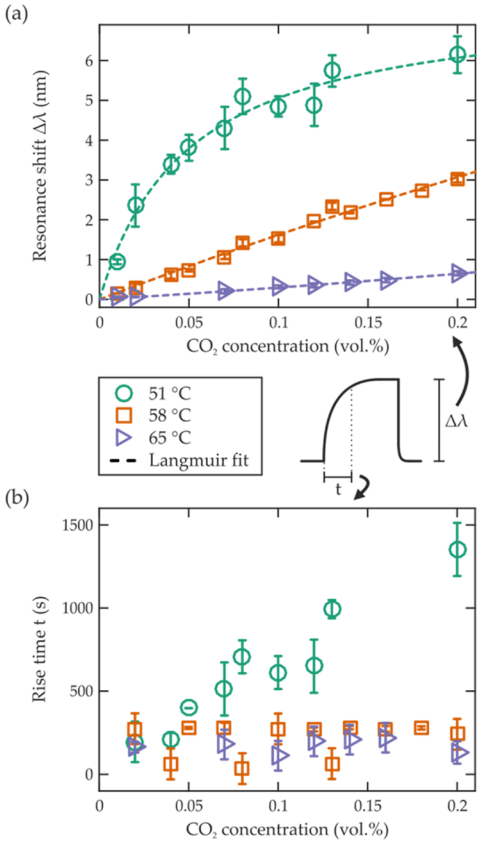

Figure 3. (a) Equilibrium resonance shift and (b) 10−90% rise time at different CO_2 concentrations and temperatures. The data points and error bars are calculated with our model of the CO_2 absorption using measurements of five different samples and a total of 102 CO_2 exposures. The dashed lines are fits of Langmuir isotherms.

the fitted model in equilibrium at different concentrations and temperatures and its standard deviation for a total of 102 CO_2 exposures measured on five different samples. The measurements were carried out by using a custom mixed test gas containing 2000 ppm CO_2 in N_2 at a constant flow rate of 1 slm.

As argued before, the resonance shift in equilibrium upon CO_2 absorption approximately follows a Langmuir isotherm. This is confirmed here, as illustrated by the dashed lines in Figure 3a. The Langmuir isotherms fit well to the concentration dependence of the resonance shift, allowing for a reliable interpolation of the resonance shift at any concentration.

The resonance shift exhibits a saturating concentration dependence at T = 51 °C, starting with a steep slope and therefore also a high sensitivity, which decreases with increasing concentration. The data points at T = 58 and 65 °C show in general a lower resonance shift but a nearly linear behavior and therefore a constant sensitivity over the measured concentration range. This leads to a higher sensitivity for low concentrations at low temperatures and a higher sensitivity for high concentrations at high temperatures, which means that it is possible to tune the sensitive concentration range by adjusting the temperature.

Figure 3b displays the rise time from 10 to 90% of the maximum shift acquired from the fits of our model to the measurements. As for the resonance shift, the model does not give accurate values above 600 s but more of an estimate of the concentration and temperature dependence. Nevertheless, the values fit well with the experiences from the experiments. While the rise time shows a clear concentration dependence at 51 °C, it is nearly constant at higher temperatures, which means that the mechanism is limiting the changes. One possible explanation is that, at higher temperatures, the delivery of CO_2 to the amines (diffusion) is the limiting factor, in contrast to the reaction speed of the amines with CO_2 at lower temperatures. This would also fit the two steps (diffusion and adsorption) of our model.

Overall, Figure 3 reveals a strong difference in the behavior of the system between 51 and 58 °C, which suggests a structural change in the PEI film and should be further investigated in future research.

As indicated in Figure 3a, it is possible to shift the sensitive concentration range by changing the temperature. This also holds true for higher concentrations. Figure 4 depicts the

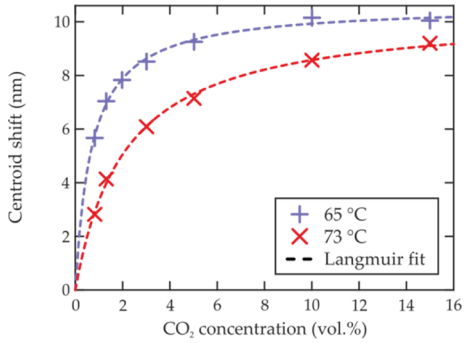

Figure 4. Resonance shift for concentrations between 1 and 15 vol % CO_2 at varying temperatures, calculated by fitting our CO_2 absorption model to the measurement data.

resonance shift at equilibrium obtained by fitting our model to the measurements at higher concentrations than Figure 3a. The other measurement parameters were kept the same as before.

The resonance shift in this concentration range still follows the same basic behavior as in Figure 3a and can be described well by Langmuir isotherms, which are indicated by the dashed lines. Even though the temperatures were increased up to T = 73 °C, still, no linearity occurs. Instead, both temperatures display a saturating behavior similar to the 51 °C data in Figure 3a. With increasing temperature, the saturation kink smears out stronger and the slope of the Langmuir isotherm at 15 vol % increases, which means that the sensitivity increases in the higher concentration range. This supports the statement from before that the sensitive concentration range is tunable by the temperature. Additionally, this indicates that the sensor is able to measure up to 100 vol % CO_2 if the temperature is increased sufficiently. Since PEI starts to decompose at 225 °C according

https://dx.doi.org/10.1021/acssensors.0c01151
ACS Sens. 2020, 5, 2628−2635

to distributor specifications, there is sufficient room to increase the temperature to measure up to 100 vol % CO_2.

On the other hand, it is possible to reach very small concentrations by decreasing the temperature at the cost of a slower rise time. To test very low concentrations, a custom test gas containing 100 ppm CO_2 in N_2 is used. The minimum gas flow rate that can be reached with the used mass flow controllers is 0.053 slm. Therefore, a stable concentration of 1.5 ppm was reached at a total flow rate of 4 slm. The humidifier was adjusted accordingly to keep the humidity constant at 0.015 g/L. Figure 5 shows the time trace of the resonance shift during a gas cycle changing from 10 to 1.5 ppm CO_2 at a temperature of 33 °C. Even though the saturation and relaxation times are quite high due to the reduced temperature and the signal does not reach a complete equilibrium, all concentrations indicate a clear resonance shift. From a comparison of the Langmuir isotherm of a previous measurement at 40 °C, which reached equilibrium much better with its corresponding noise level, a theoretical detection limit of 400 ppb CO_2 is estimated (see Figure S6).

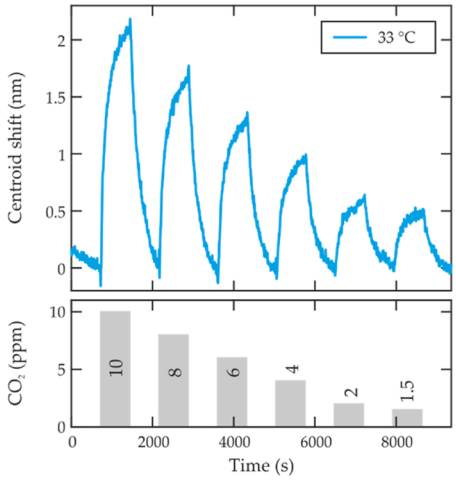

Figure 5. Time series of the resonance centroid shift at 33 °C and 0.015 g/L absolute humidity during the gas cycle varying from 10 ppm CO_2 down to 1.5 ppm.

DEGRADATION AND CROSS SENSITIVITIES

The amines in PEI can degrade by either oxidation or by urea formation. In the first case, oxygen reacts with the amines and forms stable amides and oximes. This reaction requires free amines and therefore cannot happen if CO_2 is bound to them. In the latter case, two amines react together with CO_2 to urea. This can be prevented by adding humidity.[51,52] To enhance the degradation resistance further, Zhai and Chuang proposed to blend the PEI with polyvinylalcohol (PVA).[53]

Heydari-Gorji and Sayari showed already that the CO_2 uptake of PEI-containing adsorbents was stable for 300 adsorption−desorption cycles at 75 °C in humid conditions.[52] To test the long-term stability of the samples, fresh samples have been fabricated and measured repeatedly with the same gas cycle (1 vol % CO_2 for 600 s at T = 51 °C) over the course of 3 weeks. Two of the samples are coated with pure PEI and one with a blend of PEI and PVA. One PEI sample was stored between the measurements in a nitrogen-flooded box, while the blended sample was stored together with the other PEI sample in ambient conditions. Figure 6a shows the development of the observed resonance shift during the different measurements. Since the samples were removed from the measurement setup after each measurement, it was not possible to measure the same position on the sample each time. Instead, care was taken to use a position with a similar reflectance spectrum each time for the individual samples.

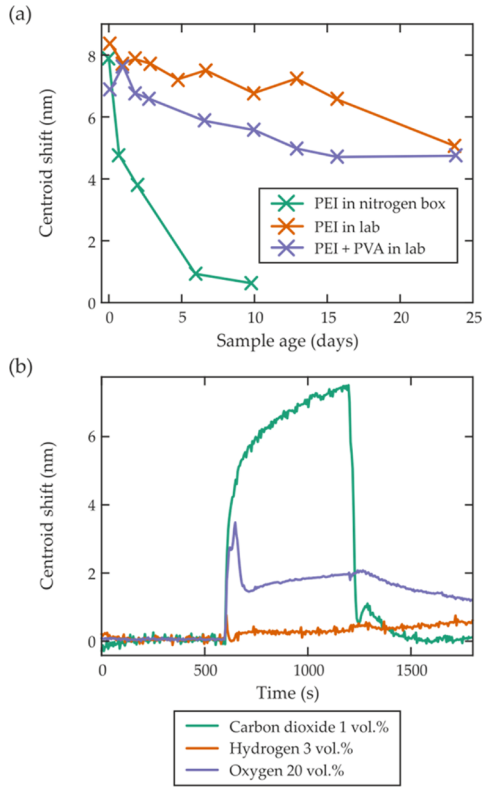

Figure 6. (a) Decrease of the resonance centroid shift of samples stored in different environments. The measurements were done each time with 1 vol % CO_2 at T = 51 °C at a comparable position on the sample. (b) Sensitivity of PEI-coated samples to 20 vol % oxygen and 3 vol % hydrogen in comparison to their response to 1 vol % CO_2 at T = 51 °C.

The sample stored in nitrogen exhibits the fastest degradation, which can be attributed to urea forming inside the PEI due to the lack of humidity. After 10 days, nearly no reaction at all is visible anymore. In contrast, the two samples stored in ambient conditions show much less degradation and are still usable after 3 weeks. Even though the sample coated with pure PEI exhibits a stronger shift in the beginning, the PEI/PVA-blend coated sample exhibits a slightly weaker slope over time. It has been shown in the literature that PEI does not react with other complex gases such as CO, NH_3, NO_2, and CH_4.[54] Figure 6b shows a time trace of the resonance shift during the exposure of a sample to different gases for 600 s each at a constant flow rate of 1 slm and a temperature of T = 51 °C. While the sample shows a strong reaction to 1 vol % CO_2, it does not respond to 3 vol % hydrogen and is much weaker to 20 vol % oxygen (all mixed with N_2). The exposure to oxygen led to a degradation of PEI and therefore to a permanent change of the resonance position and a weaker response to CO_2. Even though the hydrogen did not influence the sample in any way, it may be possible to trigger a methylation of the amines using the gold disks as a catalyst.[55] The peaks at 600 s result from a short instability of the gas mixing system due to the switching of the gas mixture.

https://dx.doi.org/10.1021/acssensors.0c01151
ACS Sens. 2020, 5, 2628−2635

CONCLUSIONS

A plasmonic perfect absorber coated with a thin film of PEI has been developed for CO_2 sensing and studied in detail. We showed that the sensor sample reacts to CO_2 by red-shifting its resonance wavelength due to the reaction of the contained amines with CO_2. The resonance shift as well as the rise time increase with increasing CO_2 concentration and decreasing temperature. The shape of a Langmuir isotherm can model the resonance shift. Furthermore, it was shown that it is possible to tune the sensitive concentration range by changing the temperature. While the humidity is kept constant in this paper, it is necessary to study the impact of different humidities in future research to fully characterize the sensor. The minimum detected concentration was 1.5 ppm CO_2 at T = 33 °C, while the lower detection limit was estimated to be as low as 400 ppb. By increasing the temperature, a concentration of 15 vol % (15.000 ppm) was measured at T = 73 °C, but the system should be able to detect up to pure CO_2 at sufficiently high temperatures. Over the course of 3 weeks, samples stored at ambient conditions showed only a slight degradation, while samples stored in nitrogen were unusable after 10 days. No cross sensitivity to hydrogen and only a small cross sensitivity to oxygen were found. This demonstrates that PEI-covered plasmonic structures offer a versatile sensor design that can access a very broad range of concentrations.

This CO_2 sensor sample can be integrated in future studies into a single wavelength sensor such as the one shown by Herkert et al. to reduce the complexity and cost of the sensor.[22] This would make the sensor even more interesting for applications where carbon dioxide is mixed with an explosive gas like in the fabrication of synthetic fuels where hydrogen is included.[56]

ASSOCIATED CONTENT

Supporting Information

The Supporting Information is available free of charge at https://pubs.acs.org/doi/10.1021/acssensors.0c01151.

> Data Processing—referencing, centroid detection, drift correction, and fitting model; measurement at room temperature; determination of the theoretical lower detection limit; and intensity change at a fixed wavelength upon CO_2 exposure (PDF)

AUTHOR INFORMATION

Corresponding Authors

Tobias Pohl − *4th Physics Institute and Research Center SCoPE, University of Stuttgart, 70569 Stuttgart, Germany;* orcid.org/0000-0003-3028-8992; Email: t.pohl@pi4.uni-stuttgart.de

Harald Giessen − *4th Physics Institute and Research Center SCoPE, University of Stuttgart, 70569 Stuttgart, Germany;* Email: giessen@pi4.uni-stuttgart.de

Authors

Florian Sterl − *4th Physics Institute and Research Center SCoPE, University of Stuttgart, 70569 Stuttgart, Germany;* orcid.org/0000-0002-1025-6777

Nikolai Strohfeldt − *4th Physics Institute and Research Center SCoPE, University of Stuttgart, 70569 Stuttgart, Germany*

Complete contact information is available at: https://pubs.acs.org/10.1021/acssensors.0c01151

Notes

The authors declare no competing financial interest.

ACKNOWLEDGMENTS

The authors gratefully acknowledge the financial support by ERC (COMPLEXPLAS), by the Baden-Württemberg Stiftung, by the Deutsche Forschungsgemeinschaft, by the Bundesministerium für Bildung und Forschung, and by the Ministerium für Wissenschaft, Forschung und Kunst Baden-Württemberg.

REFERENCES

(1) British Petroleum *BP Statistical Review of World Energy 2019 | 68th Edition*; British Petroleum, 2019; Vol. *68*.

(2) Fox, C. G.; Alder, J. F. Surface Acoustic Wave Sensors for Atmospheric Gas Monitoring a Review. *Analyst* **1989**, *114*, 997−1004.

(3) Harren, F. J. M.; Mandon, J.; Cristescu, S. M. Photoacoustic Spectroscopy in Trace Gas Monitoring. In *Encyclopedia of Analytical Chemistry*; John Wiley & Sons, Ltd: Chichester, UK, 2012.

(4) Azad, A. M. Solid-State Gas Sensors: A Review. *J. Electrochem. Soc.* **1992**, *139*, 3690.

(5) Krebs, P.; Grisel, A. A Low Power Integrated Catalytic Gas Sensor. *Sens. Actuators, B* **1993**, *13*, 155−158.

(6) Bakker, E.; Telting-Diaz, M. Electrochemical Sensors. *Anal. Chem.* **2002**, *74*, 2781−2800.

(7) Guth, U.; Vonau, W.; Zosel, J. Recent Developments in Electrochemical Sensor Application and Technology - A Review. *Meas. Sci. Technol.* **2009**, *20*, No. 042002.

(8) Eguchi, K. Optical Gas Sensors. In *Gas Sensors*; Springer Netherlands: Dordrecht, 2011; pp. 307−328.

(9) Hodgkinson, J.; Tatam, R. P. Optical Gas Sensing: A Review. *Meas. Sci. Technol.* **2013**, *24*, No. 012004.

(10) Bogue, R. Detecting Gases with Light: A Review of Optical Gas Sensor Technologies. *Sens. Rev.* **2015**, *35*, 133−140.

(11) Tardy, P.; Coulon, J. R.; Lucat, C.; Menil, F. Dynamic Thermal Conductivity Sensor for Gas Detection. *Sens. Actuators, B* **2004**, *98*, 63−68.

(12) de Graaf, G.; Abarca Prouza, A.; Ghaderi, M.; Wolffenbuttel, R. F. Micro Thermal Conductivity Detector with Flow Compensation Using a Dual MEMS Device. *Sens. Actuators, A* **2016**, *249*, 186−198.

(13) Kühnemann, F. Photoacoustic Detection of CO2. In *Carbon Dioxide Sensing*; Gerlach, G., Guth, U., Oelßner, W., Eds.; John Wiley & Sons, Ltd, 2019; pp. 191−213.

(14) Scholz, L.; Perez, A. O.; Knobelspies, S.; Wöllenstein, J.; Palzer, S. MID-IR LED-Based, Photoacoustic CO2 Sensor. *Procedia Eng.* **2015**, *120*, 1233−1236.

(15) Huber, J.; Weber, C.; Eberhardt, A.; Wöllenstein, J. Photoacoustic CO2-Sensor for Automotive Applications. *Procedia Eng.* **2016**, *168*, 3−6.

(16) Chu, W.-F.; Fischer, D.; Erdmann, H.; Ilgenstein, M.; Köppen, H.; Leonhard, V. Thin and Thick Film Electrochemical CO2 Sensors. *Solid State Ionics* **1992**, *53-56*, 80−84.

(17) Mardare, D.; Adomnitei, C.; Florea, D.; Luca, D.; Yildiz, A. The Effect of CO2 Gas Adsorption on the Electrical Properties of Fe Doped TiO2 Films. *Phys. B* **2017**, *524*, 17−21.

(18) Wetchakun, K.; Samerjai, T.; Tamaekong, N.; Liewhiran, C.; Siriwong, C.; Kruefu, V.; Wisitsoraat, A.; Tuantranont, A.; Phanichphant, S. Semiconducting Metal Oxides as Sensors for Environmentally Hazardous Gases. *Sens. Actuators, B* **2011**, *160*, 580−591.

(19) Neethirajan, S.; Jayas, D. S.; Sadistap, S. Carbon Dioxide (CO2) Sensors for the Agri-Food Industry - A Review. *Food Bioprocess Technol.* **2009**, *2*, 115−121.

(20) European Commission. *ATEX 2014/34/EU Guidelines*; 2nd ed.; European Commission, 2017.

(21) Martin, P. E.; Barker, E. F. The Infrared Absorption Spectrum of Carbon Dioxide. *Phys. Rev.* **1932**, *41*, 291−303.

(22) Herkert, E.; Sterl, F.; Strohfeldt, N.; Walter, R.; Giessen, H. Low Cost Hydrogen Sensor in the ppm Range with Purely Optical Read-Out. *ACS Sens.* **2020**, 978.
(23) Wadell, C.; Syrenova, S.; Langhammer, C. Plasmonic Hydrogen Sensing with Nanostructured Metal Hydrides. *ACS Nano* **2014**, *8*, 11925−11940.
(24) Tittl, A.; Mai, P.; Taubert, R.; Dregely, D.; Liu, N.; Giessen, H. Palladium-Based Plasmonic Perfect Absorber in the Visible Wavelength Range and Its Application to Hydrogen Sensing. *Nano Lett.* **2011**, *11*, 4366−4369.
(25) Liu, N.; Mesch, M.; Weiss, T.; Hentschel, M.; Giessen, H. Infrared Perfect Absorber and Its Application As Plasmonic Sensor. *Nano Lett.* **2010**, *10*, 2342−2348.
(26) Ameling, R.; Giessen, H. Microcavity Plasmonics: Strong Coupling of Photonic Cavities and Plasmons. *Laser Photon. Rev.* **2013**, *7*, 141−169.
(27) Sterl, F.; Strohfeldt, N.; Both, S.; Herkert, E.; Weiss, T.; Giessen, H. Design Principles for Sensitivity Optimization in Plasmonic Hydrogen Sensors. *ACS Sens.* **2020**, 917.
(28) Griessen, R.; Strohfeldt, N.; Giessen, H. Thermodynamics of the Hybrid Interaction of Hydrogen with Palladium Nanoparticles. *Nat. Mater.* **2016**, *15*, 311−317.
(29) Teutsch, T.; Strohfeldt, N.; Sterl, F.; Warsewa, A.; Herkert, E.; Paone, D.; Giessen, H.; Tarin, C. Mathematical Modeling of a Plasmonic Palladium-Based Hydrogen Sensor. *IEEE Sens. J.* **2018**, *18*, 1946−1959.
(30) Qin, J.; Chen, Y. H.; Ding, B.; Blaikie, R. J.; Qiu, M. Efficient Plasmonic Gas Sensing Based on Cavity-Coupled Metallic Nanoparticles. *J. Phys. Chem. C* **2017**, *121*, 24740−24744.
(31) Mayer, K.; Hafner, J. H. Localized Surface Plasmon Resonance Sensors. *Chem. Rev.* **2011**, *111*, 3828−3857.
(32) Langhammer, C.; Larsson, E. M.; Kasemo, B.; Zorić, I. Indirect Nanoplasmonic Sensing: Ultrasensitive Experimental Platform for Nanomaterials Science and Optical Nanocalorimetry. *Nano Lett.* **2010**, *10*, 3529−3538.
(33) Liu, N.; Tang, M. L.; Hentschel, M.; Giessen, H.; Alivisatos, A. P. Nanoantenna-Enhanced Gas Sensing in a Single Tailored Nanofocus. *Nat. Mater.* **2011**, *10*, 631.
(34) Shen, X.; Du, H.; Mullins, R. H.; Kommalapati, R. R. Polyethylenimine Applications in Carbon Dioxide Capture and Separation: From Theoretical Study to Experimental Work. *Energy Technol.* **2017**, *5*, 822−833.
(35) Doan, T. C. D.; Baggerman, J.; Ramaneti, R.; Tong, H. D.; Marcelis, A. T. M.; van Rijn, C. J. M. Carbon Dioxide Detection with Polyethylenimine Blended with Polyelectrolytes. *Sens. Actuators, B* **2014**, *201*, 452−459.
(36) Hasan, D.; Lee, C. Hybrid Metamaterial Absorber Platform for Sensing of CO2 Gas at Mid-IR. *Adv. Sci.* **2018**, *5*, 1700581.
(37) Nugroho, F. A. A.; Xu, C.; Hedin, N.; Langhammer, C. UV-Visible and Plasmonic Nanospectroscopy of the CO2 Adsorption Energetics in a Microporous Polymer. *Anal. Chem.* **2015**, *87*, 10161−10165.
(38) Ko, Y. G.; Shin, S. S.; Choi, U. S. Primary, Secondary, and Tertiary Amines for CO2 Capture: Designing for Mesoporous CO2 Adsorbents. *J. Colloid Interface Sci.* **2011**, *361*, 594−602.
(39) Choi, S.; Drese, J. H.; Jones, C. W. Adsorbent Materials for Carbon Dioxide Capture from Large Anthropogenic Point Sources. *ChemSusChem* **2009**, *2*, 796−854.
(40) Vaidya, P. D.; Kenig, E. Y. Acceleration of CO2 Reaction with N,N-Diethylethanolamine in Aqueous Solutions by Piperazine. *Ind. Eng. Chem. Res.* **2008**, *47*, 34−38.
(41) Kim, S.; Shi, H.; Lee, J. Y. CO2 Absorption Mechanism in Amine Solvents and Enhancement of CO2 Capture Capability in Blended Amine Solvent. *Int. J. Greenhouse Gas Control* **2016**, *45*, 181−188.
(42) Weiss, T.; Gippius, N. A.; Tikhodeev, S. G.; Granet, G.; Giessen, H. Derivation of Plasmonic Resonances in the Fourier Modal Method with Adaptive Spatial Resolution and Matched Coordinates. *J. Opt. Soc. Am. A* **2011**, *28*, 238.
(43) Walter, R.; Tittl, A.; Berrier, A.; Sterl, F.; Weiss, T.; Giessen, H. Large-Area Low-Cost Tunable Plasmonic Perfect Absorber in the near Infrared by Colloidal Etching Lithography. *Adv. Opt. Mater.* **2015**, *3*, 398−403.
(44) Dahlin, A. B.; Tegenfeldt, J. O.; Höök, F. Improving the Instrumental Resolution of Sensors Based on Localized Surface Plasmon Resonance. *Anal. Chem.* **2006**, *78*, 4416−4423.
(45) Le Chatelier, H. Sur Un Énoncé Général Des Lois Des Équilibres Chimiques. *C.-R. Acad. Sci.* **1884**, *99*, 786−789.
(46) Weiss, T.; Mesch, M.; Schäferling, M.; Giessen, H.; Langbein, W.; Muljarov, E. A. From Dark to Bright: First-Order Perturbation Theory with Analytical Mode Normalization for Plasmonic Nanoantenna Arrays Applied to Refractive Index Sensing. *Phys. Rev. Lett.* **2016**, *116*, 237401.
(47) Warren, J. R.; Gordon, J. A. On the Refractive Indices of Aqueous Solutions of Urea. *J. Phys. Chem.* **1966**, *70*, 297−300.
(48) Zhu, T.; Yang, S.; Choi, D. K.; Row, K. H. Adsorption of Carbon Dioxide Using Polyethyleneimine Modified Silica Gel. *Korean J. Chem. Eng.* **2010**, *27*, 1910−1915.
(49) Paul, D. R. Gas Sorption and Transport in Glassy Polymers. *Ber. Bunsengesellschaft Phys. Chem.* **1979**, *83*, 294−302.
(50) Crank, J. *The Mathematics of Diffusion*; Oxford University Press, 1975, 1267.
(51) Sayari, A.; Belmabkhout, Y. Stabilization of Amine-Containing CO2 Adsorbents: Dramatic Effect of Water Vapor. *J. Am. Chem. Soc.* **2010**, *132*, 6312−6314.
(52) Heydari-Gorji, A.; Sayari, A. Thermal, Oxidative, and CO2-Induced Degradation of Supported Polyethylenimine Adsorbents. *Ind. Eng. Chem. Res.* **2012**, *51*, 6887−6894.
(53) Zhai, Y.; Chuang, S. S. C. Enhancing Degradation Resistance of Polyethylenimine for CO2 Capture with Cross-Linked Poly(Vinyl Alcohol). *Ind. Eng. Chem. Res.* **2017**, *56*, 13766−13775.
(54) Srinives, S.; Sarkar, T.; Hernandez, R.; Mulchandani, A. A Miniature Chemiresistor Sensor for Carbon Dioxide. *Anal. Chim. Acta* **2015**, *874*, 54−58.
(55) Du, X.-L.; Tang, G.; Bao, H.-L.; Jiang, Z.; Zhong, X.-H.; Su, D.-S.; Wang, J.-Q. Direct Methylation of Amines with Carbon Dioxide and Molecular Hydrogen Using Supported Gold Catalysts. *ChemSusChem* **2015**, *8*, 3489−3496.
(56) Probstein, R. F.; Hicks, R. E. *Synthetic Fuels*; Dover Publications, 2006.

https://dx.doi.org/10.1021/acssensors.0c01151
ACS Sens. 2020, 5, 2628−2635